Computing the effective diffusivity using a spectral method

Jingzhi Zhu [a,*], Long-Qing Chen [a], Jie Shen [b], Veena Tikare [c]

[a] *Department of Materials Science and Engineering, 119 Steidle Building, Penn State University, University Park, PA 16802, USA*
[b] *Department of Mathematics, Penn State University, University Park, PA 16802, USA*
[c] *Materials Modeling and Simulation, Sandia National Laboratory, Albuquerque, NM 87185-1411, USA*

Abstract

We developed a numerical method for computing the effective properties of a microstructure. The method is particularly efficient and accurate for microstructures with a diffuse-interface description similar to those generated from phase-field simulations. In particular, we considered the diffusive transport property of a microstructure by solving the steady-state diffusion equation using a Fourier–Chebyshev spectral method. Computed effective diffusivities agree very well with existing analytical solutions and computer simulations for a number of simple model systems. Combining with the phase-field model for simulating microstructure evolution, the proposed method can be applied for modeling the temporal evolution of effective properties. This is illustrated by considering grain growth and the corresponding effective transport property evolution as function of time. © 2001 Elsevier Science B.V. All rights reserved.

Keywords: Effective diffusivity; Diffuse interface; Diffusion equation; Spectral method; Microstructures

1. Introduction

The effective properties of a heterogeneous material such as a composite or a polycrystalline ceramics depend not only on the volume fractions and the properties of each individual component, but also critically on the details of a material microstructure. For macroscopically homogeneous microstructures, property bounds can be obtained from a statistical description via a variety of n-point correlation functions (see e.g. Refs. [1,2]). However, the exact property of a specific microstructure has to be computed numerically except for special cases with very simple microstructures for which analytical solutions exist. For example, by using finite difference or finite element methods, Garboczi and Bentz developed a package for calculating the effective linear electric and elastic properties of a microstructure generated either from digitization of experimental data or from a microstructure simulation model [3]. In the finite difference or finite element methods, the local property of a material is assumed to change

discontinuously across the interfaces separating different phases or domains. Another approach to obtain the effective properties of a material is to use direct computer simulations. For example, to calculate the effective diffusion coefficient of a microstructure, Monte Carlo techniques can be employed to simulate the distance traveled by the tracers in a certain amount of walker diffusion time [4,5].

Recently, we modeled the diffusive transport process in a microstructure by solving the time-dependent diffusion equation using the semi-implicit Fourier–Chebyshev spectral method [6]. The microstructures employed in the calculation were usually generated by a phase-field model. It was shown that with temporal diffusion profiles, the effective diffusivity of a microstructure may be extracted from a given concentration profile at a particular time.

The purpose of this paper is to present a method to compute the effective diffusivity of a microstructure by directly solving the steady-state diffusion equation using a spectral method. The method is particularly efficient and accurate for microstructures described by diffuse interfaces, for which current software packages such as those developed by Garboczi cannot be directly applied. In combination with a phase-field approach,

* Corresponding author. Tel.: +1-814-865-0389; fax: +1-814-865-0016.

E-mail address: jzhu@psu.edu (J. Zhu).

the proposed model allows us to simulate the effective diffusivity evolution of a material as a function of time during a microstructural evolution process. Moreover, we want to point out that although the focus of this paper is on computing effective properties of a microstructure with a diffuse-interface description, the numerical method discussed here can be applied for modeling microstructure evolution in systems with multi-rate processes when one or more of the processes are essentially at steady-state or slaved by the slowest process.

2. Numerical methods

To model the diffusion process of a given atomic species through a heterogeneous material, we used the so-called space-dependent field variables to describe the microstructure of the material, similar to the phase-field approach [7]. The field variables represent the spatial distribution of different phases or domains. The composition difference throughout the microstructure can be described by a compositional field. The structural difference between domains/phases is usually described by long-range order parameters. For example, a single-phase polycrystalline microstructure can be represented by a set of continuous orientation field variables, $\eta_1(r), \eta_2(r), \ldots, \eta_p(r)$, where p is the number of grain orientations in the system [7,8]. Instead of using the conventional sharp-interface description of a microstructure, we used a diffuse-interface model, where the field variables are continuous across the phase/domain boundaries and interfaces. One important advantage of the diffuse-interface model is that it avoids the specification of boundary conditions at those interfaces.

The spatial dependence of diffusivity is introduced through its dependence on the field variables, i.e., we describe the diffusivity $D(r)$ as a function of field variables. For example, for a single-phase polycrystalline microstructure, we expressed the diffusivity D in a scaled form as $D = D^* \left(1 - a\Sigma_{i=1}^{p} \eta_i^2 \right)$, where D^* and a are positive constants. The values of $\Sigma\eta_i^2$ in the grain bulk are higher than those in the grain boundaries, and therefore the fact that grain boundary diffusivity D_{gb} is higher than grain bulk diffusivity D_v is easily shown from this simple equation. Changing the value of a allows us to obtain different ratios of D_{gb}/D_v. The difference between grain boundary diffusion coefficient and grain bulk diffusion coefficient in our simulation can be as large as four to five orders of magnitude. Although the choice of diffusivity/field variable relationship was quite arbitrary, we found it would not significantly affect the general results in predicting the effective property. The diffuse-interface approach also results in a continuous property change across the grain

boundaries or phase interfaces. Consequently, we do not have to specify the boundary conditions at the interfaces between different regions with different diffusivities. However, it should be pointed out that the diffusivity throughout the microstructure is not required to be continuous across interfaces as they are in the phase-field model. Examples with a sharp-interface model as well as a diffuse-interface model are presented to compare our results with analytical solutions and some other numerical methods.

Consider the diffusion in a heterogeneous material when a concentration gradient of a diffusing species is applied to maintain a steady mass transport. For the steady-state diffusion problem, where the diffusive flux is steady in time, the diffusion equation can be written as

$$\nabla \cdot [D(r)\nabla C(r)] = 0, \tag{1}$$

where $D(r)$ is the diffusivity (or diffusion coefficient) and $C(r)$ is the concentration distribution on a given microstructure. Isotropic diffusivities are considered in our work. Given $C(r)$, the flux $J(r)$ can be easily calculated by Fick's first law $J(r) = -D(r)\nabla C(r)$. We consider a two-dimensional system with a periodic boundary condition in the x-direction and a fixed boundary condition in the y-direction which has fixed diffusant source and sink. The effective diffusivity D_{eff}, which was defined simply in terms of the averages of various diffusivities over the system, is then obtained from the relation $\langle J \rangle = -D_{eff}\nabla C$, where $\langle J \rangle$ is the average of the flux at each node in a discretized version of Eq. (1).

Finite difference or finite element methods are most commonly used to numerically solve Eq. (1). These methods are generally easy to implement but their effectiveness is limited by their low accuracy [9]. Spectral methods, which have been widely used in computational fluid dynamics [10], however, are accurate and efficient alternatives for solving partial differential equations, especially when the underlying computational domains are rectangular. For simulating microstructure evolution, rectangular domains are always used. The diffuse nature of the interfaces also makes the spectral method very useful for dealing with microstructures in our model. Recently, we used a semi-implicit Fourier spectral method to solve the time-dependent Cahn–Hilliard [11] and diffusion equation [6]. Significant gains in computing time and memory were observed by using a high-order spectral scheme, compared with conventional finite difference and finite element methods. Thus, we propose a spectral approach here to solve the steady-state diffusion equation with the underlying boundary conditions.

We consider a rectangular computational domain $[0,2\pi) \times [-1,1]$. Any other domain size can be studied similarly by simple coordinate transformations. The boundary conditions are

$$C(x, -1) = 0, C(x, 1) = 1$$

for all $x \in [0, 2\pi]$; C is periodic in x. (2)

The fixed boundary condition represents a constant diffusant source and sink at both surfaces in y-direction. If we denote $u(x, y) = C(x, y) - \dfrac{1 + y}{2}$, then u satisfies a homogeneous Dirichlet boundary condition in y. Denoting $f(r)$ as the term $\nabla \cdot \left[D(r) \nabla \left(\dfrac{1 + y}{2} \right) \right]$, we are led to consider

$$- \nabla \cdot [D(r) \nabla u(r)] = f(r), \tag{3}$$

$$u(x, \pm 1) = 0 \quad \text{for all } x \in [0, 2\pi],$$

u is periodic in x.

We now describe briefly a Fourier–Chebyshev method for solving the above equation. Generally speaking, spectral methods look for an approximation of the unknown function $u(x, y)$ as an expansion of a set of globally smooth basis functions. More precisely, we choose the trignometric polynomials $\phi(x) = e^{ijx}$ for the periodic x-direction and Chebyshev polynomials $T_k(y)$ in the y-direction. Therefore, we look for the approximate solution $u_N(x, y)$ for Eq. (3) in the form

$$u_N(x, y) = \sum_{j = -N/2}^{N/2} \sum_{k = 0}^{N-2} u_{j,k} e^{ijx} [T_k(y) - T_{k+2}(y)], \tag{4}$$

where $u_{j,k}$ are called the expansion coefficients in the frequency space. Since $T_k(\pm 1) = (\pm 1)^k$, we have $T_k(\pm 1) - T_{k+2}(\pm 1) = 0$ and therefore $u_N(x, \pm 1) = 0$. The boundary conditions are then satisfied. This set of convenient basis functions was first used in [12] and offers many computational advantages. In fact, we can solve Eq. (3) by using the spectral method at a cost comparable to the finite difference/finite element methods with the same number of grid points. See Ref. [12] for more details.

Let us denote X_N to be a set, where all the functions in X_N has a form of Eq. (4) with the expansion coefficients satisfying $\bar{u}_{j,k} = u_{-j,k}$. Here $\bar{u}_{j,k}$ is the complex conjugate of $u_{j,k}$. Such a condition ensures that functions in X_N are real valued. We used a Galerkin approach that based on variational formulations using continuous inner products [10]. More specifically, we need to find $u_N \in X_N$ such that

$$- (\nabla \cdot [D(r) \nabla u_N(r)], v_N)_\omega = (I_N f(r), v_N)_\omega,$$

for all $v_N \in X_N$, (5)

where the inner product $(\cdot, \cdot)_\omega$ is defined as

$$(u, v)_\omega = \int_0^{2\pi} dx \int_{-1}^1 u(x, y) v(x, y) (1 - y^2)^{-1/2} \, dy,$$

and I_N is the interpolation operator based on the spectral-collocation points [10]. The above variational formulation leads to a linear system of the form

$$A_N \bar{u} = \bar{f}, \tag{6}$$

where $\bar{u}$ and $\bar{f}$ are the vectors formed by the unknowns $u_{j,k}$ and the right-hand side function f, respectively. However, A_N is a full and ill-conditioned matrix that makes Eq. (6) difficult to solve. Hence, we propose a preconditioned iterative method to solve this linear system.

The main idea is that if there exist numbers α, $\beta > 0$, such that $\alpha \leqslant D(x, y) \leqslant \beta$ for all (x, y), which is the case for most applications, then the elliptic operator $- (\nabla \cdot D(r) \nabla)$ is spectrally equivalent to the Laplacian operator $- \Delta$. Thus, we can use the linear system associated to $- \Delta$ as a preconditioner for Eq. (6). More precisely, we consider the Fourier–Chebyshev Galerkin method for the Poisson equation

$$- (\Delta u_N(r), v_N)_\omega = (I_N f(r), v_N)_\omega, \quad \text{for all } v_N \in X_N. \tag{7}$$

Similarly, the above system leads to a linear system

$$B_N \bar{u} = \bar{f}. \tag{8}$$

Thus, instead of solving Eq. (6) which is ill-conditioned, we solve the equivalent preconditioned system

$$B_N^{-1} A_N \bar{u} = B_N^{-1} \bar{f}. \tag{9}$$

The fact that $- (\nabla \cdot D(r) \nabla)$ is spectrally equivalent to $- \Delta$ implies that the condition number of $B_N^{-1} A_N$ will be independent of N, and only depend on the ratio β/α. Thus, a suitable iterative method, for example the Conjugate Gradient Squared (CGS, [13]), applied to Eq. (9) will converge quickly if the ratio β/α is within a certain range. The large the ratio β/α is, the more number of iterations is needed for converging. We found that Eq. (9) converged very fast if $\beta/\alpha < 10$.

We note that to apply CGS to Eq. (9), we only need to carry out the following two types of operations:
1. Given $\bar{u}$, compute $A_N \bar{u}$;
2. Given $\bar{f}$, compute $\bar{u}$ by solving $B_N \bar{u} = \bar{f}$.

We emphasize that there is no need to compute explicitly the entries of A_N and that the product $A_N \bar{u}$ can be computed in $O(N^2 \log N)$ operations by using FFT. On the other hand, Eq. (8) can also be solved in $O(N^2 \log N)$ operations as described in [12]. Thus, overall, Eq. (6) can be solved in $O(N^2 \log N)$ operations.

3. Results and discussion

By numerically solving the steady-state diffusion equation with variable coefficient, we can obtain the steady-state concentration profile throughout the microstructure for any diffusivity distribution $D(r)$. To test our numerical algorithm, exactly solvable problems involving a continuous variation of $D(r)$ were examined. We have tested a few simple cases, where the diffusivity distribution depends only on y, i.e.,

$D(x,y) = D(y)$. Diffusional transport is then one-dimensional and thus the exact steady-state diffusion equation can be easily solved [14]. Fig. 1 shows a few examples of computed concentration distribution along y. Our computed values agree exactly with the analytical solutions. For example, curve C, the plot of computed $C(x,y)$ when $D(y) = y + 2$, matches exactly the analytically derived concentration profile $C_a(x,y) = \ln(y + 2)/\ln 3$.

The effective diffusivity is then calculated from the steady-state flux. For the one-dimensional diffusion problem considered above, the effective diffusivity can be analytically derived from the Reuss bound: $\dfrac{1}{D_{\text{eff}}} = $
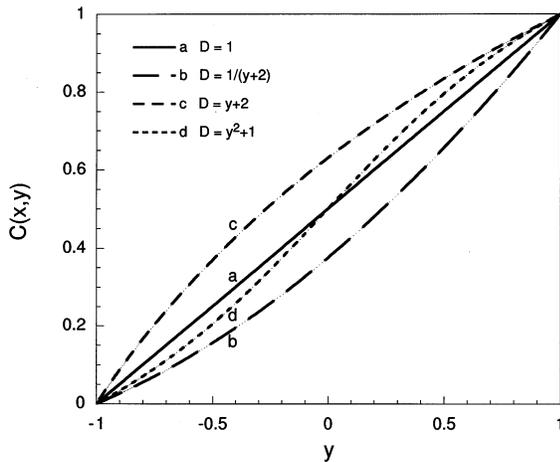

Fig. 1. Computed steady-state concentration distribution along y-direction when the diffusivity distribution depends only on y. $C_a(x,y)$ is the analytical solution for different $D(y)$. Computed $C(x,y)$ agree exactly with $C_a(x,y)$. (a) $D = 1$, $C_a(x,y) = (1 + y)/2$; (b) $D = 1/(y + 2)$, $C_a(x,y) = (y^2/8) + (y/2) + (3/8)$; (c) $D = y + 2$, $C_a(x,y) = (\ln(y + 2))/(\ln 3)$; (d) $D = y^2 + 1$, $C_a(x,y) = (2/\pi) \tan^{-1}(y) + (1/2)$.
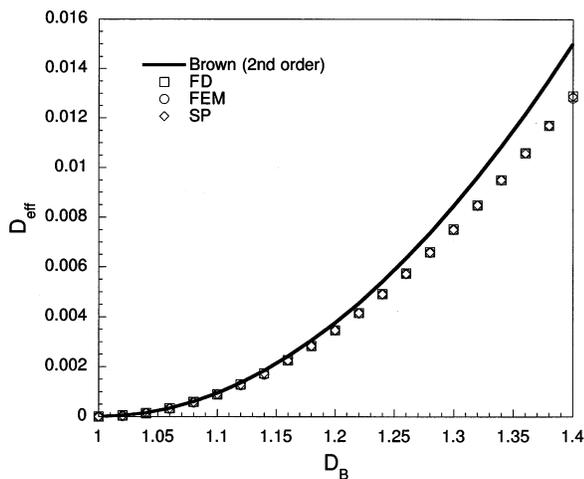

Fig. 2. D_{eff} as a function of D_B for a microstructure with a small contrast of the diffusivities $D_A = 1.0$. The quantity $D_A + V_B(D_B - D_A)$ was subtracted from both numerical and analytical results.

$\Sigma_i \dfrac{V_i}{D_i}$, where V_i and D_i are the volume fraction and diffusivity of each component [15]. However, a continuous version needs to be used here considering the continuous nature of the diffusivity distribution, i.e., $\dfrac{2}{D_{\text{eff}}} = \int_{-1}^{1} \dfrac{dy}{D(y)}$. For $D(y) = y + 2$, the analytic $D_{\text{eff}} = 2/\ln 3$. Our computed D_{eff} from the average steady-state flux is 1.8204784532614, with an error $< 10^{-10}$ to the analytic value $2/\ln 3$. For other types of $D(y)$ in Fig. 1, excellent agreement was also observed between the computed and analytically derived effective diffusivity. Therefore, high accuracy is achieved by using our spectral methods.

Spectral methods are most efficiently applied to problems with smooth changes in the variables and the coefficients, which are generally not easy to approach by conventional finite difference and finite element methods. However, from our numerical experiments, we find that our spectral methods also yield reasonably accurate results even for systems with sharp interfaces. As test examples, we have compared our numerical computations with exact analytical solutions for a few very special microstructures.

We first consider a two-phase system, where the property difference between the two phases is small. In this case, the effective property can be expressed as a power series expansion in terms of this difference [1,16]. For example, for a general two-dimensional microstructure, it was shown by Brown et al. that the effective diffusivity was written as [17]

$$D_{\text{eff}} = D_A + V_B(D_B - D_A) - \frac{1}{2} V_A V_B \frac{(D_B - D_A)^2}{D_A}$$
$$+ O(D_B - D_A)^3 + \dots \qquad (10)$$

In a second order approximation, the coefficients for the $O(D_B - D_A)^3$ and higher order terms, which involve details of the microstructure, can be omitted if the property difference is sufficiently small. Following the work of Garboczi [17], we tested our program with a 100×100 pixel square (phase B) centered in a 256×256 lattice as the microstructure. It is very convenient for us to carry out comparisons between our spectral computations and their FEM and FD results. Fig. 2 shows one example of such a comparison for a microstructure with a small contrast between two phase diffusivities, where D_{eff} was plotted against D_B. D_A is set to be 1. Here a sharp-interface description was used in our spectral methods, NIST's finite difference method and NIST's finite element method. The quantity $D_A + V_B (D_B - D_A)$ was subtracted from both numerical and analytical results. Our numerical data agree very well with the FEM and FD results although different boundary conditions were employed in their programs. As the difference between D_A and D_B becomes larger, the difference between numerical results
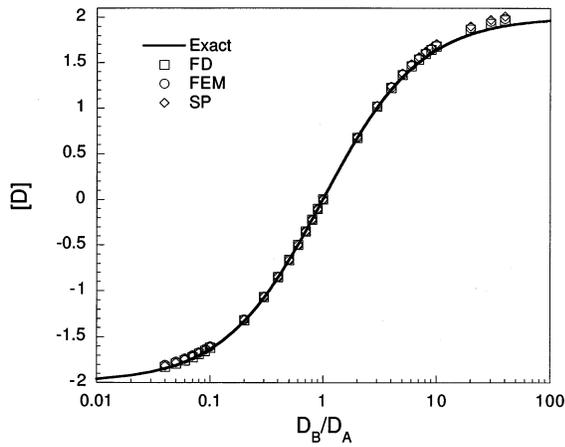
Fig. 3. Intrinsic diffusivity [D] for a circle embedded in a square matrix as a function of the two phase diffusivity ratio, D_B/D_A, SP, FEM, FD and the analytical results are compared.

and Brown's second-order analytical results becomes larger due to the contributions from the cubic term in Eq. (10).

The effective property of a dilute mixture can be derived analytically in a power series in terms of the volume fraction of the second phase. For example, for particles of phase B randomly distributed in a matrix (phase A) with a small volume fraction, the effective property can be written as [17,18]

$$\frac{D_{\text{eff}}}{D_A} = 1 + [D]V_B + O(V_B^2). \tag{11}$$

The term [D] in the above equation is called the intrinsic property, which is a function of the shape of the particle and the contrast between its property D_B and the property of the matrix D_A. For circular particles in two-dimensional, the intrinsic property is given by

$$[D] = \frac{2(D_B - D_A)}{D_A + D_B}. \tag{12}$$

We put a circular particle with a radius 25 centered on the middle of a square 256×256 lattice ($V_B \approx 3\%$). Diffusivity has a discontinuous change (sharp interface) across the circle interface. The intrinsic property was plotted against the ratio of diffusivity D_B/D_A, shown in Fig. 3. Good agreement was achieved between the FD and FEM results, which were obtained from computer programs developed by NIST, and our spectral computation results. All the numerical data are close to the solid line, which was the exact solution from Eq. (12) when D_B/D_A is within the range $0.1 \sim 10$. However, when D_B is significantly different from D_A, the difference between numerical results and theoretical predictions becomes large. It would be expected that smaller volume fraction could improve the result.

The above examples demonstrate that even for systems with a sharp-interface description, the proposed

spectral method can produce reasonably accurate results as compared with previous FD and FEM calculations as well as with analytical solutions. The spectral method is particularly effective for smooth interfaces in a microstructure described by the phase-field model. As an example, we consider the evolution of the effective diffusivity for a single-phase polycrystalline material during a grain growth process. We have utilized a diffuse-interface field model for modeling microstructure evolution processes such as spinodal decomposition, Ostwald ripening, and grain growth [7]. By combining the phase-field simulation of microstructural evolution with our spectral method for computing effective property, we are able to obtain not only the mesoscale morphological pattern evolution, but also the effective property evolution from the time-dependent microstructures.

As discussed previously, an arbitrary single-phase polycrystalline microstructure was described by a large set of continuous nonconserved orientation field variables which distinguish the different orientations of grains. Their values change continuously from 0 to 1. According to the diffuse-interface theory, the total free energy of an inhomogeneous system can be written as [19]

$$F = \int\int \left[f_0(\eta_1(r), \eta_2(r), \ldots, \eta_p(r)) + \sum_{i=1}^{p} \frac{\kappa_i}{2}(\nabla\eta_i(r))^2 \right] dV, \tag{13}$$

where f_0 is the local free energy depending on field variables, and grain boundary energy is represented by the second term in the above integral. κ is the gradient energy coefficient. The spatial and temporal evolution of the orientation field variables is described by Ginzburg–Landau equations

$$\frac{d\eta_i(r,t)}{dt} = -L_i \frac{\delta F}{\delta\eta_i(r,t)}, \tag{14}$$

where L_i are the kinetic coefficients related to grain boundary mobility, t is time and F is the total free energy. With a proper chosen local free energy form f_0, Eq. (14) can be solved efficiently by a semi-implicit Fourier spectral method [9].

An example of a grain growth process from a two-dimensional simulation is shown in Fig. 4, where 36 nonconserved field variables were introduced. The microstructure was represented by $\Sigma\eta_i(r)^2$, which were displayed by gray levels with low and high values represented by dark and bright colors. The initial values of η_i were essentially zero with a small perturbation. After a short time, a well-defined grain structure formed. Further grain growth was driven by the reduction of grain boundary energy, resulting in an increase of average grain size.

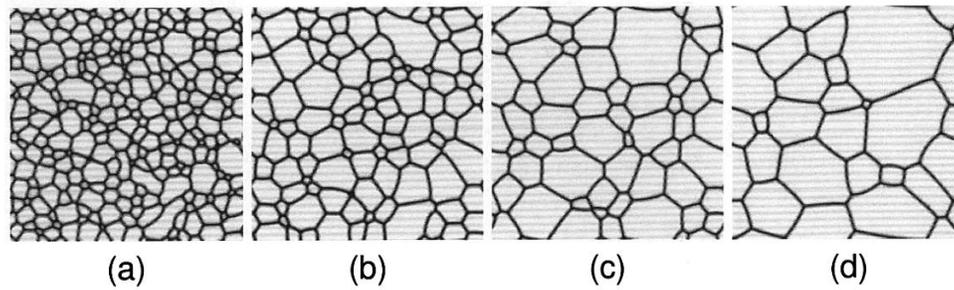The computation of the effective properties at different times can be performed by applying a concentration

Fig. 4. The microstructure evolution during a single-phase grain growth displayed by $\Sigma \eta_i^2$ (36 nonconserved orientation field variables η_i were used): (a) $t = 200$; (b) $t = 1000$; (c) $t = 2000$; (d) $t = 4000$.

gradient across the corresponding microstructure. Assuming the diffusion atoms do not interact with the polycrystalline media, we compute the effective diffusivity by inputting the microstructure into Eq. (1) by relating $D(r)$ with $\Sigma \eta_i(r)^2$. Fig. 5 shows an example of D_{eff} evolving as a function of time. At later times, as the grain size becomes larger, the volume fraction of grain boundaries decreases, resulting a decrease in the effective diffusion coefficient. In Fig. 5, we also plotted the theoretical effective diffusivities D_{upper} and D_{lower} as the upper and lower bounds, which were predicted by first order series and parallel bounds (or called Voigt and Reuss bounds), as $D_{\text{gb}}f_{\text{gb}} + D_{\text{v}}(1 - f_{\text{gb}})$ and $D_{\text{gb}}D_{\text{v}}/[D_{\text{gb}}(1 - f_{\text{gb}}) + D_{\text{v}}f_{\text{gb}}]$, respectively, where f_{gb} is the volume fraction of grain boundaries. However, for a diffuse-interface description of the microstructure, there is some ambiguity in determining the exact values of the diffusivity of grain boundary D_{gb}, the diffusivity of grain bulk D_{v} and f_{gb}. Recognizing that D_{eff} predicted by Voigt and Reuss bounds is essentially a volume average, we calculated D_{upper} as $\frac{1}{N} \Sigma_r D(r)$, where N is the total number of lattice points. Similarly D_{lower} was computed as $N / \left[\Sigma_r 1/D(r) \right]$. As expected, for all the grain sizes studied, D_{eff} is between D_{upper} and D_{lower}, which are the effective diffusivities for idealized grain structures, where grain boundaries can be treated as parallel slabs embedded in the grains. These results are generally in good agreement with our previous simulation results from solving a time-dependent diffusion equation [6].

4. Conclusion

We applied an efficient and accurate spectral method to compute the effective diffusivity for any arbitrary microstructures. The method is particularly effective and accurate for systems with smooth and diffuse interfaces. Even for systems with sharp interfaces with jumps in the property across the interfaces, the pro-

posed method produces good results as compared to previous FD and FEM calculations as well as analytical solutions. In combination with the phase-field modeling of microstructure evolution, the proposed method allows us to study both the microstructure evolution and the effective diffusivity evolution. Our methods can be used to calculate other effective physical properties, such as thermal conductivity and electrical conductivity, if we recognize that the equations describing the steady-state or equilibrium are essentially the same. Moreover, the proposed approach can be utilized for studying a general class of problems involving rate processes with different time scales, where one of the processes is essentially at steady-state or in equilibrium.
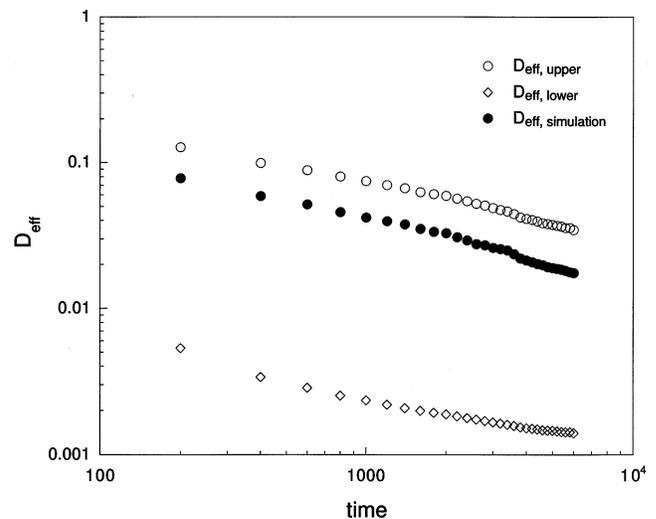
Fig. 5. Effective diffusivity D_{eff} evolution as a function of time during a single-phase grain growth. Filled circles are from our simulations. Open circles and diamonds represent the effective diffusivities predicted by mixtured rules.

References

[1] S. Torquato, Appl. Mech. Rev. 44 (1991) 37.

[2] S. Torquato, Int. J. Solids Struct. 35 (1998) 2385.

[3] E.J. Garboczi, D.P. Bentz, Constr. Buildg. Mater. 10 (1996) 293.

[4] M.R. Riley, F.J. Muzzio, H.M. Buettner, S.C. Reyes, Phys. Rev. E 49 (1994) 3500.

[5] C.D. Siclen, Phys. Rev. E 59 (1999) 2804.

[6] J. Zhu, L.Q. Chen, J. Shen, V. Tikare, Comput. Mat. Sci. 20 (2001) 37.

[7] L.Q. Chen, Y.Z. Wang, JOM 48 (1996) 13.

[8] D.N. Fan, L.Q. Chen, S.P. Chen, Mater. Sci. Eng. A238 (1997) 78.

[9] L.Q. Chen, J. Shen, Comput. Phys. Commun. 108 (1998) 147.

[10] C. Canuto, M.Y. Hussaini, A. Quarteroni, T.A. Zang, Spectral Methods in Fluid Dynamics, Springer, Berlin, 1987.

[11] J. Zhu, L.Q. Chen, J. Shen, V. Tikare, Phys. Rev. E 60 (1999) 3564.

[12] J. Shen, SIAM J. Sci. Comput. 16 (1995) 74.

[13] P. Sonneveld, SIAM J. Sci. Stat. Comput. 10 (1989) 86.

[14] J. Crank, The Mathematics of Diffusion, Oxford University Press, London, 1975.

[15] C.W. Nan, Prog. Mater. Sci. 37 (1993) 1.

[16] W.F. Brown, J. Chem. Phys. 23 (1955) 1514.

[17] E.J. Garboczi, Finite Element and Finite Difference Programs for Computing the Linear Electric and Elastic Properties of Digital Images of Random Materials, NISTIR 6269, http://ciks.cbt.nist.gov/garboczi/.

[18] E.J. Garboczi, J.F. Douglas, Phys. Rev. E 53 (1996) 6169.

[19] J.W. Cahn, J.E. Hilliard, J. Chem. Phys. 28 (1958) 258.